Geophys. J. Int. (2014) **199,** 1677–1681
GJI Seismology
doi: 10.1093/gji/ggu327

EXPRESS LETTER

Seismic attenuation: effects of interfacial impedance on wave-induced pressure diffusion

Qiaomu Qi,[1] Tobias M. Müller[2] and J. Germán Rubino[3]

[1]*Department of Exploration Geophysics, Curtin University, Perth, WA* 6151, *Australia. E-mail: qiaomu.qi1@postgrad.curtin.edu.au*
[2]*Mineral Resources Flagship, CSIRO, Perth, WA* 6151, *Australia*
[3]*Applied and Environmental Geophysics Group, University of Lausanne, CH*-1015 *Lausanne, Switzerland*

Accepted 2014 August 22. Received 2014 August 21; in original form 2014 July 12

SUMMARY

Seismic attenuation and dispersion in layered sedimentary structures are often interpreted in terms of the classical White model for wave-induced pressure diffusion across the layers. However, this interlayer flow is severely dependent on the properties of the interface separating two layers. This interface behaviour can be described by a pressure jump boundary condition involving a non-vanishing interfacial impedance. In this paper, we incorporate the interfacial impedance into the White model by solving a boundary value problem in the framework of quasi-static poroelasticity. We show that the White model predictions for attenuation and dispersion substantially change. These changes can be attributed to petrophysically plausible scenarios such as imperfect hydraulic contacts or the presence of capillarity.

Key words: Seismic attenuation; Wave propagation; Acoustic properties.

1 INTRODUCTION

Nearly 40 years ago White *et al.* (1975) presented a model for seismic *P*-wave attenuation and dispersion for a periodically stratified medium with alternating gas–water layers. The underlying attenuation mechanism is controlled by pressure diffusion as a consequence of wave-induced pressure gradients across the layers. Not only because of the relevance of partially saturated sediments for exploration seismology, but also because of the insightful physical arguments they used, their work continues to trigger research into wave propagation in porous media. The White model has been reproduced within the framework of Biot's theory of poroelasticity (Biot 1962) using a different approach (Norris 1993). It has been subsequently specialized in order to analyse the effects of random layering (Gurevich & Lopatnikov 1995; Müller & Gurevich 2004), inhomogeneous rock properties (Carcione & Picotti 2006) and embedded fractures with variable infill (Kong *et al.* 2013). The White model has been generalized to account for dissipation associated with pressure diffusion at the wavelength scale (Kudarova *et al.* 2013) and obliquely incident *P* and *SV* waves (Krzikalla & Müller 2011).

Key to the White model is the definition of a representative elementary volume (REV) encompassing the gas–water interface (Fig. 1). At this interface the continuity of the fluid pressure is assumed to hold throughout the fluid pressure equilibration process, that is, from the onset of wave-induced fluid pressure gradients to the final constant pressure once equilibrium is reached. This interface condition is chosen in accordance with the open-pore boundary condition of Deresiewicz & Skalak (1963). The latter is, however, an end-member of a more general, sometimes called natural boundary condition, wherein the pressure jump across the interface is proportional to the relative fluid–solid velocity (Bourbié *et al.* 1987). This pressure jump boundary condition can be related to petrophysically plausible scenarios (Dutta & Odé 1979). One is associated with a perturbed hydraulic contact across the interface, as it may arise in the presence of non-load-bearing clay minerals clogging the pore throats (Fig. 1). A second scenario is related to the presence of macroscopic capillarity, thereby creating a permanent pressure jump (Nagy & Blaho 1994). Therefore, the question arises how this pressure jump boundary condition alters the predictions of the White model. From analogous problems in thermal diffusion it is known that this kind of jump boundary conditions can significantly alter the effective conductivity of heterogeneous structures (Cheng & Torquato 1997). Given that the White model is heavily used to interpret seismic attenuation estimates (e.g. Morgan *et al.* 2012), any significant changes may possibly entail important implications. Indeed, previous works indicate that the pressure jump boundary condition associated with capillary action reduces seismic attenuation (Tserkovnyak & Johnson 2003; Markov & Levin 2007; Qi *et al.* 2014).

The aim of this paper is to incorporate the pressure jump boundary condition into the White model in a general fashion so that both aforementioned scenarios (and possibly other scenarios) can be modelled. To do so, we argue that the proportionality coefficient of the pressure jump boundary condition can be interpreted as an interfacial impedance. This interfacial impedance captures the

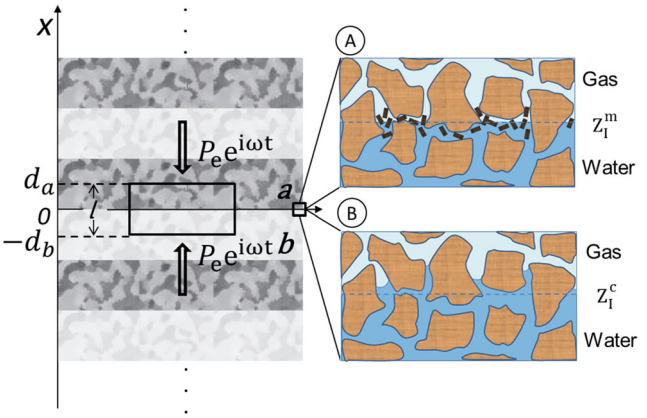

Figure 1. Schematic representation of a homogeneous sandstone alternatively saturated by water and gas layers. The sketch at pore scale shows two possible interface scenarios: (a) clay minerals are clogging the hydraulic contact and (b) menisci unevenly distributed due to capillarity.

particular interface properties that cannot be assigned to the gas- or water-saturated layer. We then solve the modified boundary value problem for the double layer geometry within the framework of quasi-static poroelasticity.

2 THEORY

2.1 Background: White model and interfacial impedance

White *et al.* (1975) determine the effective, frequency-dependent *P*-wave modulus $\tilde{H}(\omega)$ for a periodically layered system composed of porous layers alternately saturated with gas and water. Their approach consists in solving a boundary value problem for the REV with spatial semi-period $l = (d_a + d_b)$, as illustrated in Fig. 1. Therein the action of the *P* wave is simulated through a harmonically oscillating compression $P_e e^{i\omega t}$. The resulting ratio of vertical component of the average strain to stress is (White *et al.* 1975; their eq. 14)

$$\frac{1}{\tilde{H}} = \frac{1}{H^{nf}} + \frac{1}{\tilde{H}^{ff}}. \tag{1}$$

Herein H^{nf} is the *P*-wave modulus when fluid exchange between consecutive layers is not permitted (hence the superscript 'nf' for no-flow), as is the case when there is not enough time for the fluid pressure to equilibrate. Thus, H^{nf} can be interpreted as the high-frequency, or unrelaxed, limit. It is obtained from Backus averaging with the individual, undrained *P*-wave moduli calculated using Gassmann's equation (Gelinsky & Shapiro 1997)

$$\frac{1}{H^{nf}} = \left\langle \frac{1}{H} \right\rangle. \tag{2}$$

The angle brackets denote the volumetric, or saturation-weighted, average $\langle x \rangle = (d_a x_a + d_b x_b)/l$. According to the Biot–Gassmann theory the undrained *P*-wave modulus is given by $H = L + \alpha^2 M$, where $L = K_0 + 4\mu/3$ is the drained *P*-wave modulus, $\alpha = 1 - K_0/K_s$ the Biot–Willis coefficient, and $M = [(\alpha - \phi)/K_s + \phi/K_f]^{-1}$ the fluid storage modulus. K_s and K_0 denote the bulk moduli of the solid grains and of the dry frame. The porosity is ϕ and the frame shear modulus is μ.

The second term of the right-hand side (RHS) of eq. (1) accounts for fluid pressure diffusion across the layers, thereby reducing the overall stiffness of the medium. As this is a transient process, $\tilde{H}^{ff}$ turns out to be complex-valued and frequency-dependent,

$$\frac{1}{\tilde{H}^{ff}} = \frac{1}{i\omega l}\frac{(B_a - B_b)^2}{Z_a - Z_b} \equiv \frac{1}{i\omega l}\frac{(\Delta B)^2}{\Delta Z}. \tag{3}$$

This interlayer flow term has a simple interpretation. The (uniaxial) Skempton coefficient *B* quantifies the fluid pressure built-up induced by the external loading P_e under undrained condition, that is, when the fluid increment ξ is zero

$$B = \frac{\partial p_f^{nf}}{\partial P_e}\Big|_{\xi=0} = \frac{\alpha M}{H}. \tag{4}$$

Only if there is a contrast in the induced fluid pressures, or equivalently $\Delta B \neq 0$, fluid pressure diffusion can take place. This diffusion process is also controlled by the impedance contrast ΔZ. Herein, the diffusional impedance is defined as the ratio of the fluid pressure associated with Biot slow *P* wave and the normal component of the relative fluid–solid velocity v_n at the interface

$$Z = \frac{p_f^{ff}}{v_n}\Big|_{x=0} = \pm\frac{\coth(k_s d)}{\kappa k_s}. \tag{5}$$

We assume that the unit normal points from layer 'b' to layer 'a'. Thus, the sign of the diffusional impedance is positive for layer 'a' and negative for layer 'b'. The impedance entails the pressure diffusion wave number associated with Biot's slow *P*-wave number. In the quasi-static approximation this wave number is $k_s \equiv \sqrt{i\omega/D_p}$ with the diffusivity $D_p = \kappa N$. Herein κ is the hydraulic conductivity given by the ratio of permeability and fluid shear viscosity and $N = M(1 - \alpha B)$. It is important to notice that eq. (5) is independent of the properties of the interface, that is, the condition of fluid pressure continuity across the boundary is not used.

From the above considerations it becomes clear that the induced fluid pressure difference across the interface is central to initiate interlayer flow. It also means that interlayer flow is sensitive to the continuity of the pressure at the interface. In Biot 's theory of poroelasticity the pressure at the interface is generally described by (Deresiewicz & Skalak 1963; Bourbié *et al.* 1987)

$$p_{fa}|_{x=0} - p_{fb}|_{x=0} = -Z_I v_n|_{x=0}. \tag{6}$$

It relates the pressure jump across the interface with the relative fluid–solid velocity. The proportionality coefficient Z_I is called the resistance coefficient. If there is no resistance, $Z_I = 0$, the layers are in perfect hydraulic contact. Then, the so-called 'open-pore boundary condition' is satisfied and the pressure is continuous across the interface. Conversely, for any finite $Z_I \neq 0$ there exists a pressure jump, whereas for $Z_I \to \infty$ no pressure equilibration can take place. In general, Z_I can be interpreted as an interfacial impedance assigning a particular property to the interface. It may even have a reactance term ($\mathrm{Im}\{Z_I\} \neq 0$), as discussed further below. In the next section, we show how this interfacial impedance can be incorporated in the derivation of an effective *P*-wave modulus.

2.2 Effective strain for finite interfacial impedance

We base the derivation on the quasi-static poroelasticity equations (Biot 1962). In the space–frequency domain they are given by

$$\frac{\partial \tau_{xx}}{\partial x} = 0, \tag{7}$$

$$\frac{\partial p_f}{\partial x} = -\frac{i\omega}{\kappa} w, \tag{8}$$

where τ_{xx} is the total stress, p_f the fluid pressure and $w = v/i\omega$ the average relative fluid displacement per unit volume of bulk material. Eqs (7) and (8) represent stress equilibrium and Darcy's law, respectively. They are coupled through the constitutive relations

$$\tau_{xx} = H\frac{\partial u}{\partial x} + BH\frac{\partial w}{\partial x}, \tag{9}$$

$$p_f = -BH\frac{\partial u}{\partial x} - M\frac{\partial w}{\partial x}, \tag{10}$$

with u being the average displacement of the solid phase.

For a homogeneous medium, eqs (7)–(10) can be combined such that the governing equation for w becomes

$$\frac{\partial^2 w}{\partial x^2} = \frac{i\omega}{D_p} w. \tag{11}$$

This means that the out-of-phase movement between the fluid and solid phases, which is associated with the Biot slow P wave, is governed by diffusion. The solution for the considered REV can be written as

$$w_i = \sum_{\gamma=1}^{2} A_{i,\gamma} \exp\{(-1)^\gamma k_{si} x\}, \quad i = a, b, \tag{12}$$

with $A_{i,\gamma}$ being complex constants. Since the equation of equilibrium (7) implies that the stress is constant throughout the REV and equal to the applied compression, $\tau_{xx} = -P_e$, we write the remaining poroelastic fields as

$$u_i = -B_i w_i - \frac{P_e}{H_i} x + E_i, \tag{13}$$

$$p_{fi} = B_i P_e - N_i \frac{\partial w_i}{\partial x}, \quad i = a, b, \tag{14}$$

where E_i are two additional unknowns. For the REV under uni-axial deformation, the resulting overall strain and the effective plane wave modulus are defined by

$$\tilde{e}_{xx} = (u_a|_{x=d_a} - u_b|_{x=-d_b})/l\,, \tag{15}$$

$$\tilde{H}(\omega) = -P_e/\tilde{e}_{xx}\,. \tag{16}$$

To uniquely determine the overall strain, another five equations are needed. These equations are obtained by choosing appropriate boundary conditions. Due to symmetry, we impose no-flow conditions at the boundaries of the REV

$$v_a|_{x=d_a} = v_b|_{x=-d_b} = 0\,. \tag{17}$$

In addition, we require continuity of solid displacement and relative fluid–solid velocity at the interface

$$u_a|_{x=0} = u_b|_{x=0}\,, \tag{18}$$

$$v_a|_{x=0} = v_b|_{x=0}\,. \tag{19}$$

The fifth boundary condition is provided by the partially open boundary condition (6). It can be written in decomposed form as

$$p_{fa}^{nf} + p_{fa}^{ff} = p_{fb}^{nf} + p_{fb}^{ff} - Z_I v_n, \quad (x = 0), \tag{20}$$

where we interpret the pressure as $p_f = p_f^{nf} + p_f^{ff}$.

The first term on the RHS of eq. (14) quantifies the fluid pressure when fluid flow across the interface is not permitted, that is, $p_{fi}^{nf} = B_i P_e$. The second term describes the effect of diffusion on the fluid pressure, that is, $p_{fi}^{ff} = -N_i \frac{\partial w_i}{\partial x}$. The associated diffusional impedance can be computed from the definition (5) by applying boundary condition (17).

Next, we compute the overall effective strain by substituting eq. (13) into (15) and making use of boundary conditions (18) and (19). We obtain

$$\tilde{e}_{xx} = \underbrace{-\left(\frac{d_a}{H_a} + \frac{d_b}{H_b}\right)\frac{P_e}{l}}_{e^{nf}} + \underbrace{\frac{B_a - B_b}{i\omega l} v_n|_{x=0}}_{\tilde{e}^{ff}}\,. \tag{21}$$

Eq. (21) for the overall strain can be understood if, similarly to the pressure decomposition, the strain is represented as the sum $\tilde{e} = e^{nf} + \tilde{e}^{ff}$. If solid and fluid phases move in-phase or, equivalently, $v = 0$, then the second term on the RHS of eq. (21) vanishes, and thus the remaining term corresponds to the effective strain associated with no-flow condition, $e^{nf} = -\langle H^{-1}\rangle P_e$. If $v \neq 0$, the overall effective strain consists of two terms, wherein the second term corresponds to the additional strain in presence of pressure diffusion, $\tilde{e}^{ff}$.

Employing eqs (5), (19) in eq. (20) yields the relative fluid-solid velocity at the interface

$$v_n|_{x=0} = -\frac{B_a - B_b}{Z_a - Z_b + Z_I} P_e\,. \tag{22}$$

This equality shows that the presence of resistance coefficient Z_I reduces the relative fluid–solid velocity. Making use of the extended relative fluid–solid velocity (22) in eq. (21), we obtain the effective strain associated with the diffusion process

$$\tilde{e}^{ff} = -\frac{(B_a - B_b)^2}{i\omega l(Z_a - Z_b + Z_I)} P_e. \tag{23}$$

The overall effective strain can now be computed via summation of the component related to no flow across the interface, e^{nf}, and the contribution produced by fluid pressure diffusion between the layers, $\tilde{e}^{ff}$.

2.3 Generalized White model

The undrained P-wave modulus is obtained by substituting the overall effective strain into eq. (16). Therefore,

$$\frac{1}{\tilde{H}} = \left\langle \frac{1}{H} \right\rangle + \frac{1}{i\omega l} \frac{(\Delta B)^2}{\Delta Z + Z_I}. \tag{24}$$

This effective, undrained P-wave modulus is the main result of this paper. The interfacial impedance appears in the denominator of the interlayer flow term and adds to the impedance contrast ΔZ. If the interfacial impedance vanishes, $Z_I = 0$, then eq. (24) reduces to the P-wave modulus given by White *et al.* (1975; their eq. 14). This shows that the fluid pressure continuity boundary condition is rooted in the White model.

This generalized White model can be used to characterize P-wave dispersion and attenuation in partially saturated media wherein the interface separating the two fluid phases possesses specific properties. As originally envisaged by Deresiewicz & Skalak (1963) the partially open boundary condition (6) models a perturbed hydraulic contact. Then the interfacial impedance is real-valued, that is, it has the character of a resistance. It will be denoted as Z_I^m. Another scenario is related to the presence of capillary forces. The pressure jump boundary condition is then (Nagy & Blaho 1994)

$$p_{fa}|_{x=0} - p_{fb}|_{x=0} = -\frac{W}{i\omega} v_n|_{x=0}, \tag{25}$$

where W (Pa m^{-1}) is the so-called membrane stiffness, which controls the capillarity reinforcement. In this representation of the pressure jump condition, the interfacial impedance is an imaginary

number, and is given by $Z_{\mathrm{I}}^{\mathrm{c}} = -\mathrm{i}\frac{W}{\omega}$. That is, it has the character of a reactance. In the following we focus on the implications on seismic attenuation and dispersion for these two scenarios.

3 ATTENUATION AND DISPERSION

Attenuation and dispersion can be obtained from eq. (24) via $Q^{-1} = \mathrm{Im}(\tilde{H})/\mathrm{Re}(\tilde{H})$ and $V_{\mathrm{P}} = [\mathrm{Re}(1/V_{\mathrm{pc}})]^{-1}$, where the complex P-wave velocity is $V_{\mathrm{pc}} = \sqrt{\tilde{H}/\bar{\rho}}$. The effective density $\bar{\rho}$ is given by the volumetric average of the grain and fluid densities. We restrict the analysis of the results to the two scenarios mentioned above. In the first case the interfacial impedance has a resistance term only, while in the second case it is given by a reactance term. The corresponding attenuation and dispersion behaviours for a gas saturation of $S = 50$ per cent are shown in Fig. 2. Here the saturation is computed according to $S_i = d_i/l$ with $l = 0.2$ m. The red and blue families of curves correspond to the resistance and reactance scenario, respectively, and the original White's prediction is indicated by the black curves. We note that in these numerical examples the White model predictions loose their validity at very high frequencies, as then the wavelength becomes comparable to the layer thickness. However, to illustrate the asymptotic characteristics, we show velocity and attenuation up to a frequency of 0.1 MHz.

Two distinct behaviours can be observed. The resistance term causes the dispersion curve to shift towards lower frequencies with increasing resistance. The dispersion window remains unchanged and is bounded by the Gassmann–Wood (GW) and Gassmann–Hill (GH) predictions. Accordingly, the attenuation peak is shifted to lower frequencies. This shifting behaviour can be understood as a consequence of the delay the imperfect hydraulic contact imposes on the pressure equilibration process. It is interesting to note that the high-frequency attenuation asymptote changes from $Q^{-1} \propto \omega^{-1/2}$ for the White's prediction to $Q^{-1} \propto \omega^{-1}$. This change in asymptotic behaviour is attributed to the fact that, in the presence of imperfect hydraulic contacts, the distance over which the pressure gradients are equilibrated has effectively increased (Müller *et al.* 2010).

The reactance term manifests differently. In this case, the pressure jump at the interface effectively reduces the wave-induced pressure gradient across the layers. Accordingly, the effects of wave-induced pressure diffusion become less pronounced so that dispersion and attenuation are reduced. In essence, the surface tension between two immiscible fluids perturbs the energy redistribution (or mode conversion process) across the interface (Markov 2009), thereby creating a change of attenuation. An increasing membrane stiffness W increases the low-frequency limiting velocity above the GW prediction. The capillarity-extended static (CS) limit is given by (Qi *et al.* 2014)

$$H_{1\mathrm{D}}^{*} = \frac{z+T}{\frac{z}{H^{\mathrm{GW}}} + \frac{T}{H^{\mathrm{GH}}}},\ z = \left\langle \frac{N}{S^2} \right\rangle,\ T = Wl\,. \tag{26}$$

We also validate the capillarity-extended model by numerically solving a boundary value problem. The numerical results displayed by circles coincide with the model prediction.

The velocity–saturation relations (VSRs) at fixed frequency (25 Hz) for both scenarios are shown in Fig. 3(top panel). It can be observed that both, the resistance and reactance terms, cause a deviation from the White's prediction towards the GH behaviour, thereby increasing the overall stiffness of the layered system. However, this is due to different reasons. In the resistance scenario, it is the shifting behaviour that is responsible for an increased velocity at fixed finite frequency. In the reactance scenario, the imposed

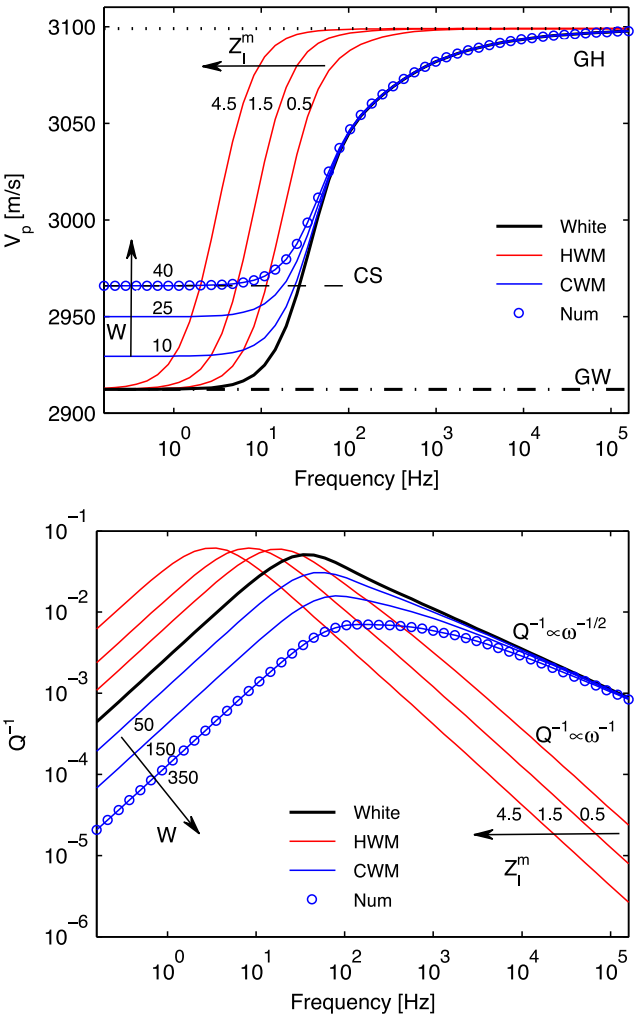

Figure 2. Phase velocity and inverse quality factor as functions of frequency for a homogeneous rock alternately saturated with gas and water. 'HWM' refers to generalized White model with imperfect hydraulic contact, whereas 'CWM' indicates the capillarity extended White model. The values of resistance $Z_{\mathrm{I}}^{\mathrm{m}}$ and membrane stiffness W are given in units of GPa · s m^{-1} and GPa m^{-1}, respectively. The parameters used in this example are: drained bulk modulus $K_0 = 7$ GPa, shear modulus $\mu = 9$ GPa, grain bulk modulus $K_{\mathrm{s}} = 35$ GPa, grain density $\rho_{\mathrm{s}} = 2650\,\mathrm{kg\,m^{-3}}$, porosity $\phi = 15$ per cent and permeability $\kappa_0 = 1\mathrm{E}-13\,\mathrm{m}^2$. The water has a bulk modulus $K_{\mathrm{fa}} = 2.25$ GPa, density $\rho_{\mathrm{fa}} = 990\,\mathrm{kg\,m^{-3}}$ and viscosity $\eta_{\mathrm{fa}} = 1\mathrm{E}-3$ Pa · s, whereas for the light gas we use $K_{\mathrm{fb}} = 0.1$ GPa, $\rho_{\mathrm{fb}} = 100\,\mathrm{kg\,m^{-3}}$ and $\eta_{\mathrm{fb}} = 3\mathrm{E}-5$ Pa · s.

pressure jump is permanent and adds to the overall stiffness. The attenuation–saturation relation (ASR) is shown in Fig. 3(bottom panel).

4 DISCUSSION AND CONCLUSION

A pressure jump boundary condition has been incorporated into the expression for the effective P-wave modulus of a partially saturated porous medium, which appears in form of an interfacial impedance (eq. 24). This generalizes the original White model wherein continuity of the fluid pressure at the gas–water interface is implicitly assumed.

Imperfect hydraulic contacts across fluid patches do not alter attenuation and dispersion in magnitude, but only decrease the characteristic frequency. Therefore, if one infers the size of fluid patches

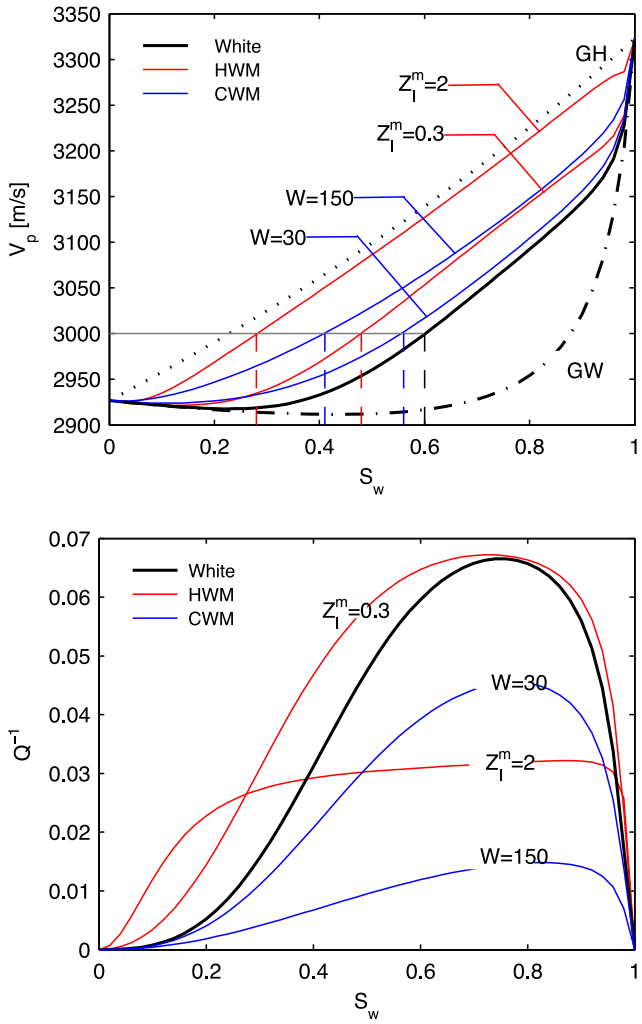

Figure 3. Velocity- and attenuation-saturation relations for a frequency of 25 Hz. The values of the resistance Z_I^m and membrane stiffness W are given in units of GPa · s m^{-1} and GPa m^{-1}, respectively.

from attenuation estimates based on the original White model, there will be a bias towards overestimating the patch size. Correspondingly, relating a measured wave velocity to saturation can result in substantial misinterpretation [e.g. in Fig. 3(top panel) the proximity to the GH bound is unrelated to the fluid patch size]. This might have important implications for understanding the role of interlayer flow in sand-shale sequences.

The effect of capillarity on inter-layer flow can be modelled by an imaginary interfacial impedance. This reactance term leads to an elevated low-frequency velocity and decrease in attenuation. Since capillary forces control the formation of fluid patches (Zhang *et al.* 2014), the generalized White model can be useful in the assessment of the corresponding acoustic signatures in laboratory settings. This is of particular interest if, in addition to fluid saturation, aligned fractures complicate the analysis of attenuation (Amalokwu *et al.* 2014).

In conclusion, the generalized White model for seismic attenuation and dispersion generates new modelling choices arising in the presence of an interfacial impedance. Although the underlying periodic double layer geometry may, in certain cases, be too simple to resemble real sedimentary records, the generalized model provides further insight into attenuation and dispersion due to interlayer flow.

REFERENCES

Amalokwu, K., Best, A.I., Sothcott, J., Chapman, M., Minshull, T. & Li, X.-Y., 2014. Water saturation effects on elastic wave attenuation in porous rocks with aligned fractures, *Geophys. J. Int.,* **197**(2), 943–947.

Biot, M.A., 1962. Mechanics of deformation and acoustic propagation in porous media, *J. appl. Phys.,* **33**(4), 1482–1498.

Bourbié, T., Coussy, O. & Zinszner, B., 1987. *Acoustics of Porous Media,* Editions Technip.

Carcione, J.M. & Picotti, S., 2006. P-wave seismic attenuation by slow-wave diffusion: effects of inhomogeneous rock properties, *Geophysics,* **71**(3), O1–O8.

Cheng, H. & Torquato, S., 1997. Effective conductivity of periodic arrays of spheres with interfacial resistance, *Proc. R. Soc. Lond., A: Math., Phys. Eng. Sci.,* **453**(1956), 145–161.

Deresiewicz, H. & Skalak, R., 1963. On uniqueness in dynamic poroelasticity, *Bull. seism. Soc. Am.,* **53**(4), 783–788.

Dutta, N. & Odé, H., 1979. Attenuation and dispersion of compressional waves in fluid-filled porous rocks with partial gas saturation (White model)—Part I: Biot theory, *Geophysics,* **44**(11), 1777–1788.

Gelinsky, S. & Shapiro, S.A., 1997. Poroelastic Backus averaging for anisotropic layered fluid-and gas-saturated sediments, *Geophysics,* **62**(6), 1867–1878.

Gurevich, B. & Lopatnikov, S., 1995. Velocity and attenuation of elastic waves in finely layered porous rocks, *Geophys. J. Int.,* **121**(3), 933–947.

Kong, L., Gurevich, B., Müller, T.M., Wang, Y. & Yang, H., 2013. Effect of fracture fill on seismic attenuation and dispersion in fractured porous rocks, *Geophys. J. Int.,* **195**(3), 1679–1688.

Krzikalla, F. & Müller, T.M., 2011. Anisotropic P-SV-wave dispersion and attenuation due to inter-layer flow in thinly layered porous rocks, *Geophysics,* **76**(3), WA135–WA145.

Kudarova, A.M., van Dalen, K.N. & Drijkoningen, G.G., 2013. Effective poroelastic model for one-dimensional wave propagation in periodically layered media, *Geophys. J. Int.,* **195**(2), 1337–1350.

Markov, M., 2009. Reflection of elastic waves at an interfaces between two porous half-spaces filled with different fluids, *Izvest., Phys. Solid Earth,* **45**(9), 769–776.

Markov, M. & Levin, V., 2007. The role of surface tension in elastic wave scattering in an inhomogeneous poroelastic medium, *Waves Random Complex Media,* **17**(4), 615–626.

Morgan, E.C., Vanneste, M., Lecomte, I., Baise, L.G., Longva, O. & McAdoo, B., 2012. Estimation of free gas saturation from seismic reflection surveys by the genetic algorithm inversion of a P-wave attenuation model, *Geophysics,* **77**(4), R175–R187.

Müller, T.M. & Gurevich, B., 2004. One-dimensional random patchy saturation model for velocity and attenuation in porous rocks, *Geophysics,* **69**(5), 1166–1172.

Müller, T.M., Gurevich, B. & Lebedev, M., 2010. Seismic wave attenuation and dispersion resulting from wave-induced flow in porous rocks—a review, *Geophysics,* **75**(5), 75A147–75A164.

Nagy, P.B. & Blaho, G., 1994. Experimental measurements of surface stiffness on water-saturated porous solids, *J. acoust. Soc. Am.,* **95**(2), 828–835.

Norris, A.N., 1993. Low-frequency dispersion and attenuation in partially saturated rocks, *J. acoust. Soc. Am.,* **94**(1), 359–370.

Qi, Q., Müller, T.M., Gurevich, B., Lopes, S.C., Lebedev, M. & Caspari, E., 2014. Quantifying the effect of capillarity on attenuation and dispersion in patchy-saturated rocks, *Geophysics,* **79**(5), WB35–WB50.

Tserkovnyak, Y. & Johnson, D.L., 2003. Capillary forces in the acoustics of patchy-saturated porous media, *J. acoust. Soc. Am.,* **114**(5), 2596–2606.

White, J.E., Mikhaylova, N. & Lyakhovitskiy, F., 1975. Low-frequency seismic waves in fluid-saturated layered rocks, *Phys. Solid Earth,* **11**(S1), 654–659.

Zhang, Y., Nishizawa, O., Kiyama, T., Chiyonobu, S. & Xue, Z., 2014. Flow behaviour of supercritical CO_2 and brine in Berea sandstone during drainage and imbibition revealed by medical X-ray CT images, *Geophys. J. Int.,* **197**(3), 1789–1807.